Effects of Solvent Flow, Dopant Flow, and Lamp Current on Dopant-Assisted Atmospheric Pressure Photoionization (DA-APPI) for LC-MS. Ionization via Proton Transfer

Damon B. Robb and Michael W. Blades
Department of Chemistry, University of British Columbia, Vancouver, British Columbia, Canada

In this paper, the effects of solvent flow, dopant flow, and lamp power on proton transfer ionization in dopant-assisted (DA) atmospheric pressure photoionization (APPI) are investigated. A broad theoretical framework is presented, describing the primary photoionization process, the formation of protonated-solvent cluster ions, and the balance between analyte ion creation via proton transfer and loss via recombination. The principal experimental test system utilized methanol as the solvent, toluene as the dopant, and acridine as the analyte. Comparisons are made between acridine and a less basic compound, 9-methylanthracene (9-MA). Experimental determinations of the trends in the analyte MH^+ signal and the total ion current (TIC) with variations in the subject parameters are provided. Experimental results and theory demonstrate that both the analyte signal and the TIC approach asymptotic limits with increases in dopant flow and/or lamp current (two factors which dictate the rate of photoion generation). The data show that these limits are lowered at higher solvent flow rates. These results are attributed to the recombination loss process, the rate of which increases with the second power of ion concentration. We deduce that the recombination rate constant increases with solvent flow rate, a consequence of the growth of ion-solvent clusters. Cluster growth is also believed to be a factor in the dramatic loss of sensitivity for 9-MA that occurs as the solvent flow is raised, because larger protonated-solvent cluster ions have greater solvation energies and may be unreactive with compounds having low gas-phase basicity and/or low solvation energy. (J Am Soc Mass Spectrom 2005, 16, 1275–1290) © 2005 American Society for Mass Spectrometry

Photoionization (PI) is the latest means of ionization to be incorporated into atmospheric pressure ionization (API) sources for liquid chromatography-mass spectrometry (LC-MS). The original motivation for the development of atmospheric pressure photoionization (APPI) sources was the demand for a method or device capable of expanding the range of compounds amenable to LC-MS to include nonpolar compounds not readily ionized by either electrospray [1, 2] or atmospheric pressure chemical ionization (APCI) [3, 4]. In recent years, two approaches towards utilizing PI at atmospheric pressure have emerged: dopant-assisted (DA) APPI [5] and direct APPI [6]. Recent review papers provide details of the two APPI-MS methods [7, 8]. This paper is concerned mainly with DA-APPI.

As is often the case for new technologies, the practical application of DA-APPI has outpaced the development of detailed knowledge regarding the mechanisms responsible for its performance. DA-APPI relies upon gas-phase ion-molecule reactions to place a charge on neutral analytes, so it is especially important that these reactions be well understood. The groups of Kostiainen and Bruins have completed several studies of the reaction chemistry of DA-APPI and the effects of solvent and dopant composition on the ionization efficiencies of different classes of compounds [9–13]. These studies have identified factors determining whether or not a particular analyte will be ionized under a given set of conditions, so that a judicious selection of solvent and dopant can be made to promote ionization of the compound of interest. For example, when the mobile phase transporting the analyte is comprised wholly or partially of either methanol or acetonitrile, and when toluene is used as a dopant, DA-APPI can deliver a proton to the analyte, provided that the analyte has a gas-phase basicity (GB) above that of the major components of the sample stream (this simple criterion ignores solvation effects, which are also a factor [14–16]; see

Published online June 23, 2005
Address reprint requests to Dr. M. W. Blades, Department of Chemistry, University of British Columbia, 2036 Main Mall, Vancouver, BC V6T 1Z1, Canada. E-mail: blades@chem.ubc.ca

1044-0305/05/$30.00
doi:10.1016/j.jasms.2005.03.017

Received February 9, 2005
Accepted March 10, 2005

Theory section, below). Under these conditions, the toluene photoions react with the solvent—through a mechanism involving the clustering of solvent around the photoions—with the result that the majority of the positive charge ultimately delivered resides with protonated solvent ions and their clusters [9, 11]. These solvent-derived ions serve as reagents for proton transfer ionization. This indirect ionization mechanism was unanticipated by the developers of DA-APPI, but it has nevertheless proven to be effective, since the sensitivity of DA-APPI utilizing proton transfer can be higher than conventional APCI [5, 17]. Charge exchange (electron-transfer) ionization of nonpolar analytes can also be effected via DA-APPI. For charge exchange to occur, the ionization energy (IE) of the analyte must be lower than the recombination energy of the dopant photoions. Further, the dopant photoions must not react with the solvent, since these reactions deplete the population of charge exchange reagents. Early experiments showed that the latter requirement could be met when using toluene dopant in combination with normal-phase solvents such as hexane, iso-octane, and chloroform [9, 11]. An important recent discovery is that anisole photoions do not react with methanol or acetonitrile, so now anisole may be utilized as a dopant to promote the ionization of nonpolar compounds under reverse-phase chromatographic conditions [13].

Notwithstanding the significant progress made to date, a number of performance characteristics of the DA-APPI source have yet to be described in the literature and/or adequately explained. One such characteristic is that the sensitivity of the method is diminished as the flow of the solvent is increased, a trend which cannot be prevented by increasing the dopant flow or the current of the discharge lamp [18]. This trend has been noted in application papers [19, 20], and in a conference presentation [21], but no study dedicated to the phenomenon has been published. A related parameter is the dopant flow rate, usually set to a value 5–10% of the solvent. This empirically-determined [18] range has become the standard for the DA-APPI method [22], though it has not been explained. Another relevant parameter is the power of the discharge lamp, which governs the rate of photon production. The commercial DA-APPI device (PhotoSpray) utilizes a DC krypton discharge lamp [23] operated at a reduced current level (~0.7 mA), roughly one-third of its maximum. This design stems from an observation made during the early development of DA-APPI: when a dopant is used, the signal does not depend strongly on the lamp current [18]. Consequently, the low current setting of the PhotoSpray source does not diminish the sensitivity of the method, while it does prolong the lifetime of the discharge lamp. To our knowledge, the (lack of) effect of lamp current has not been explained or documented in the literature.

This investigation regards proton transfer ionization in DA-APPI. The first objective is to establish a documentary record of the effects of solvent flow, dopant flow, and lamp current on the analyte ionization efficiency of the method, as well as on the total ion current (TIC) delivered. Accordingly, the experiments described here have been designed to identify and illustrate performance trends characteristic of DA-APPI, not to test hypotheses regarding fundamental mechanisms. Nevertheless, an extensive literature describing physical processes relevant to DA-APPI does exist. From this literature, and our own experience, we have constructed a theoretical framework describing the operative mechanisms of the method. A second objective of this study is, then, to present this theory, for discussion of the results at hand and as a basis for future investigations.

Experimental

Chemicals

The principal test system utilized methanol as the solvent, toluene as the dopant, and acridine (GB = 940.7 kJ mol^{-1}) as the analyte. (Note: all GB values in this paper are from reference [24]). Select experiments were repeated using acetonitrile as the solvent and 9-methylanthracene (9-MA, GB = 865.8 kJ mol^{-1}) as the analyte. Acridine and 9-MA were from Sigma-Aldrich (Oakville, Ontario, Canada). Methanol, acetonitrile, and toluene were from Fisher Scientific (Ottawa, Ontario, Canada). All solvents were HPLC grade. All chemicals were used as received.

Sample Preparation

Stock solutions of 10^{-2} M were prepared for acridine and 9-MA in methanol and acetonitrile, respectively. The acridine stock solution was diluted to make separate 10 μM solutions in each of methanol and acetonitrile. The 9-MA stock solution was diluted to make separate 50 μM solutions in each of methanol and acetonitrile.

Instrumentation

The analyte solution, solvent, and dopant were delivered separately via syringe pumps from Harvard Apparatus (Holliston, MA). The analyte solution and solvent make-up flow were combined in a tee before delivery into the ion source. For each of the experiments, the analyte solution was introduced at a fixed rate, so that the mass flow rate of analyte was constant even if the solvent flow was varied. For the parametric survey experiments, the following analyte solution flow rates were used: 3 μl min^{-1} for acridine, providing a mass flow of 30 pmol min^{-1}, and 2 μl min^{-1} for 9-MA, providing a mass flow of 100 pmol min^{-1}. For full-scan spectra (excluding the dopant-only experiments), the analyte solutions were introduced at 20 μl min^{-1} for acridine and 10 μl min^{-1} for 9-MA, while the total solvent flow rate was 200 μl min^{-1}.

The DA-APPI source was a PhotoSpray source from MDS Sciex (Concord, Ontario, Canada). This PhotoSpray source is based upon a design originally described for MDS Sciex's API 100/300/3000 series of mass spectrometers [5]. [Note that a new, significantly altered version of the PhotoSpray source has recently been introduced by MDS Sciex, for use with its API 4000/5000 instruments. In the new design, no field-free conduit has been provided between the vaporizer, the primary PI region, and the inlet of the MS. This change affects the DA-APPI method in a number of ways, so comparisons between the two source designs must be made with caution.] A schematic of the PhotoSpray source is provided in Figure 1. The distance between the PI region and the exit of the vapor conduit is about 3 cm, and the diameter of the conduit is 0.7 cm. The control unit provided with the Photospray source was not used because it did not allow the lamp current to be varied; instead, the ion source was powered by a custom HV supply (Electrical Services Shop, Chemistry Department, UBC) that allowed the lamp current to be varied between about 0.2 and 2 mA, in steps of 0.2 mA. A setting of 0.8 mA was used for those experiments not including lamp current as a variable. The offset voltage applied to the source block and transfer tube was fixed at 1.5 kV for all the MS experiments (curtain plate at 1.0 kV) and 0.5 kV for the ion current measurements (curtain plate at 0 V).

The heater around the quartz tube of the vaporizer was powered and controlled via a variable transformer. The temperature of the heater was monitored via the vaporizer's built-in thermocouple and a model HH502 thermometer from Omega (Stamford, CT). The power to the heater was manually adjusted to maintain the desired heater temperature. The temperature of the vapor exiting the conduit of the ion source was measured in separate experiments using a second thermocouple, with the ion source removed from the mass spectrometer. For methanol and acetonitrile, at liquid flow rates ranging from 25 to 1000 μl min^{-1}, the vapor temperature at the source exit varied over a small range ($\pm\sim$15 °C), centered around 200 °C for heater T = 400 °C, and 250 °C for heater T = 500 °C. Unless otherwise noted, the heater temperature was fixed at 400 °C.

For all the experiments, the total volumetric flow rate of the vapor was fixed at 7.0 l min^{-1}, at the temperature and pressure (assumed to be 760 torr) of the vapor exiting the source. By so doing, because the mass flow rate of analyte was also held constant, the number density of the analyte within the vapor was fixed. This also ensured a constant transport/reaction period within the conduit ($\sim$10 ms for these conditions). To maintain constant total volumetric flow, the auxiliary gas flow was adjusted to compensate for differences in the volume of gas produced by vaporization of varying flows of solvent and dopant. The flow rates of the nebulizer and lamp gases were fixed at 1.0 l min^{-1} (at STP). Ideal gas behavior was assumed for each component of the vapor. The auxiliary gas set point was redetermined for each solvent flow rate and each heater temperature. Model 810C mass flow controllers from Sierra Instruments (Monterey, CA) were used to set the flow rates of the lamp, nebulizer, and auxiliary gases. Pre-purified grade nitrogen from Praxair (Mississauga, Ontario, Canada) was used for all the gases.

The mass spectrometer used was a prototype single-quadrupole instrument from MDS Sciex (circa 1995). The vacuum interface and ion optics path of this instrument are closely related to those of subsequent API 100 series instruments. The housing of the PhotoSpray source was compatible with the vacuum interface of the MS and could be directly mounted without modifica-

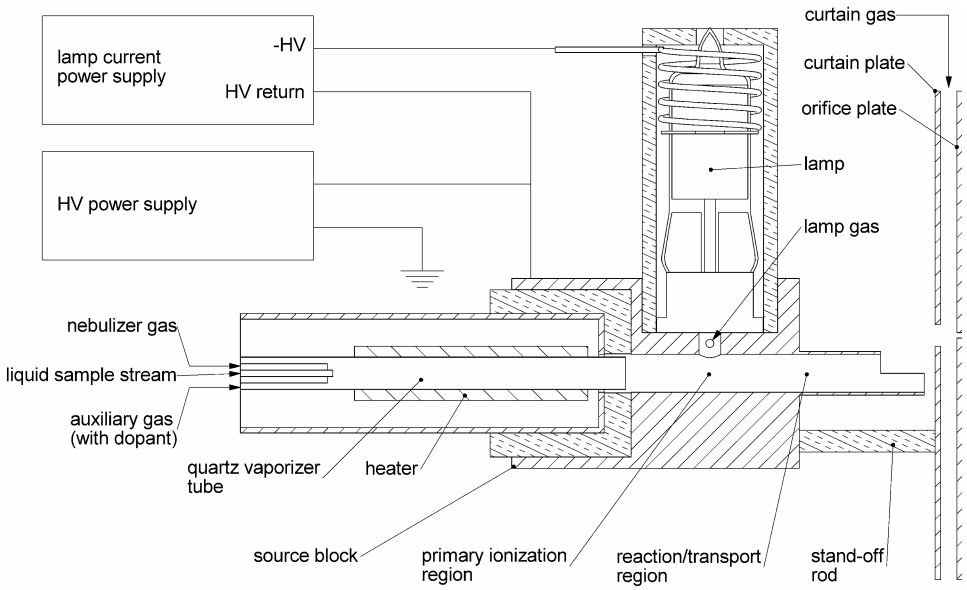

Figure 1. Schematic of DA-APPI source.

tion. For acridine, the optimal orifice plate (OR) and focusing ring (RNG) voltages were 50 and 220 V, respectively, whereas for 9-MA they were 30 and 150 V. These values were used for all experiments besides the full scan acquisitions, for which OR and RNG were set to 10 and 50 V, to minimize collision-induced dissociation. For the parametric surveys, the measured quantity was the height of the peak due to the protonated-analyte. The scan ranges for acridine and 9-MA were 179-181 and 192–194 Da, respectively. The step size was 0.1 Da and the dwell time was 50 ms. Each data point presented here is the mean determined from 60 scans. For all the full scan spectra, the scan range was 20–400 Da, the step size was 0.1 Da, the dwell time was 1 ms, and the mean of 10 scans is presented. The resolution of the quadrupole was set so that the peak width at half-height was ~0.6 Da across the mass range of interest.

The total ion current (TIC) delivered by the Photo-Spray source was also determined in a number of experiments. Knowledge of the TIC allows calculation of the terminal number density of charged particles in the vapor, since the TIC is equal to the product of the volumetric flow rate and the charge density. The TIC determinations are based upon the measurement of positive ions impinging upon the curtain plate, and they require that all ions emitted from the source be discharged on the curtain plate. The current measurements were made with a model 427 current amplifier from Kiethley Instruments (Cleveland, OH) and a model TDS 340A digital oscilloscope from Tektronix (Wilsonville, OR). The gain on the current amplifier was 10^8 V A^{-1}, and the risetime was 100 ms. Each data point is the mean of 1000 samples acquired over a period of 10 s on the oscilloscope. The 500 V potential difference between the ion source and the curtain plate was the same as that used during the regular MS experiments, so the electric field between the source and the curtain plate was consistent between the two groups of experiments. The orifice plate voltage was set to +50 V, so that there was a potential minimum at the curtain plate, and no positive ions escaped detection.

Theory

Photoionization

In the DA-APPI source under investigation here, the liquid sample stream and dopant are vaporized, then delivered via a conduit to the PI region, where the mixture is irradiated through a side-channel by the adjacent krypton discharge lamp ($h\nu$ = 10.0 and 10.6 eV). The dopant (D) has IE < $h\nu$, and usually the solvent (S) has IE > $h\nu$. Irradiation of the vapor results in direct PI of the dopant, as well as photoexcitation of the dopant and the solvent:

$$D + h\upsilon \rightarrow D^{+\cdot} + e^- \quad (1)$$

$$D + h\upsilon \rightarrow D^* \quad (2)$$

$$S + h\upsilon \rightarrow S^* \quad (3)$$

The carrier gas (nitrogen) is assumed to be transparent to the VUV photons, and the analyte and solvent additives are assumed to be at concentrations low enough so that their contribution to the absorption of the photons can be ignored. From the Beer-Lambert law, it can be shown that the rate of photon absorption by the dopant, I_D (photons s^{-1}), is given by

$$I_D = I_0 \frac{\sigma_D\ n_D}{\sigma_D\ n_D + \sigma_S\ n_S}\left\{1 - e^{-x(\sigma_D n_D + \sigma_S n_S)}\right\} \quad (4)$$

where x = distance across the ionization region (cm), I_0 = incident light intensity (photons s^{-1}), σ_D = absorption cross section for D (Mb, 1 Mb = 10^{-18} cm^2), n_D = number density of D (cm^{-3}), σ_S = absorption cross section for S (Mb), and n_S = number density of S (cm^{-3}). To convert eq 4 into the rate of dopant ion production, the fate of the excited-state intermediates, D*, must first be considered: predissociation, fluorescence, collisional quenching, and autoionization may all occur [25–27]. Since not every photon absorbed by the dopant causes ionization, we introduce a term, ϕ_T (ions $photon^{-1}$), for the total quantum yield of ionization, which encompasses the efficiencies of direct photoionization of D, as well as autoionization of D*. We assume ϕ_T is independent of n_D; according to one theory, however, ϕ_T may be a decreasing function of n_S, due to the potential role of the solvent as a collisional quenching agent [26]. The primary rate of dopant ion generation, R_P (ions s^{-1}), is then

$$R_P = \frac{dD^{+\cdot}}{dt} = I_D \phi_T \quad (5)$$

From eqs 4 and 5, predictions can be made regarding the effects of the dopant flow, solvent flow, and lamp power on the primary rate of ion generation. Starting with the simple dopant-only case, where no sample stream is introduced, eqs 4 and 5 show that R_P is expected to increase monotonically with n_D as dopant is added, with the rate of increase diminishing at high n_D, as I_D approaches I_0. Regarding the solvent, for a constant rate of dopant introduction, I_D/I_0 will always be lowered by increasing the solvent flow rate. Conversely, I_D/I_0 is expected to increase continuously as more dopant is added, for a given solvent flow rate. It is clear then that I_D/I_0 should be independent of the solvent flow rate, provided the ratio of dopant to solvent is held constant (and assuming all the incident photons are absorbed). Thus, R_P is expected to be independent of solvent flow for the standard operating conditions of DA-APPI, where the dopant flow is set to a fixed percentage of the solvent. Deviations from this ideal behavior will occur in the event that quenching of

D* by the solvent becomes a significant process, so that ϕ_T is reduced at higher solvent flows. Lastly, it is expected that R_P will be directly proportional to I_0.

In a separate suite of experiments, through the use of an ionization detector, we have measured the primary ion current generated via photoionization of dopant (toluene), in the presence of solvent (methanol), as a function of lamp current [27, 28]. Our observations are essentially consistent with the expectations derived from eqs 4 and 5, with the notable addition that ϕ_T appears to *increase* with the rate of solvent and dopant flow, though this deduction has not been verified. In any event, this work established that for a given solvent flow additional primary ion current can always be generated by raising either the dopant flow or the lamp current. Hence, a decrease in primary ion production, due to collisional quenching of D* by the solvent, is not believed to be the mechanism responsible for the observed loss of sensitivity at high solvent flows.

Ion-Molecule Reactions

Following PI of the dopant, a series of ion-molecule reactions take place which may ultimately effect analyte ionization. These reactions occur throughout the period in which the vapor resides in the field-free transport tube (~10 ms, depending upon the total volumetric flow rate of the vapor).

If the solvent contains a polar component such as methanol, acetonitrile, or water, then one rapid process is successive clustering of polar solvent molecules around the dopant photoions:

$$D^{+\cdot} + S \leftrightarrow D^{+\cdot}(S) \quad (6a)$$

$$D^{+\cdot}(S)_{n-1} + S \leftrightarrow D^{+\cdot}(S)_n \quad (6b)$$

Equation 6a is the first step in the clustering process, while 6b represents an exchange equilibrium. The forward rates of these reactions are expected to be very fast, since the number density of the solvent is large and the product clusters are stabilized by three-body collisions at atmospheric pressure. Assuming the clustering reactions are second-order and collision limited (i.e., $k_6 \approx 10^{-9}$ cm^3 s^{-1} [14, 29]), calculations of the half-lives of the clustering reactions, using typical values of n_S, indicate that an equilibrium distribution of cluster sizes is expected to be established within microseconds. The relative abundance of each cluster size is determined by the number density of the solvent, the binding strength of the solvent monomer with each cluster, and temperature.

Prior work has shown clustering to be a factor in the generation of protonated solvent ions from toluene dopant photoions [9, 11]. This phenomenon—transfer of a proton from toluene photoions to solvent neutrals having lower proton affinity (PA)—has been attributed to the presence of solvent clusters that have PAs significantly higher than those of the individual monomers [11]. From the findings of Kebarle et al. [14–16], we propose a scheme for these reactions that expressly includes the solvation energies of the clustering process:

$$D^{+\cdot}(S)_n + S \leftrightarrow SH^+(S)_m + (n-m)S + (D-H)^{\cdot} \quad (7)$$

$$\Delta G_7^\circ = GB[(D-H)^{\cdot}] - GB(S) + \Delta G^\circ_{0,m}(SH^+) - \Delta G^\circ_{0,n}(D^{+\cdot}) = -RT\ln K_7 \quad (8)$$

where ΔG_7° and K_7 are the free-energy change and the equilibrium constant for eq 7. The solvation clustering free energies, $\Delta G^\circ_{0,n}$ and $\Delta G^\circ_{0,m}$, are defined by eq 9:

$$D^{+\cdot} + n(S) \rightarrow D^{+\cdot}(S)_n \quad \Delta G^\circ_{0,n}(D^{+\cdot}) \quad (9a)$$

$$SH^+ + m(S) \rightarrow SH^+(S)_m \quad \Delta G^\circ_{0,m}(SH^+) \quad (9b)$$

It is expected that eq 7 will also reach equilibrium within microseconds, again, because of the high number density of solvent molecules in the vapor. For the simple no clustering case ($n = m = 0$), eq 8 shows that eq 7 will only proceed if GB(S) is greater than GB[(D − H)$^{\cdot}$]. Hence, unsolvated toluene photoions are not expected to undergo proton transfer reactions with methanol (GB = 724.5 kJ mol^{-1}), acetonitrile (GB = 748 kJ mol^{-1}), or water (GB = 660 kJ mol^{-1}), since these are all less basic than the benzyl radical (GB = 800.7 kJ mol^{-1}) [24]. In the DA-APPI source, though, methanol and acetonitrile do react with toluene photoions [9]. We propose that the energy required to make eq 7 exoergic for toluene photoions with methanol and acetonitrile is supplied from the difference in solvation energies between the clusters $D^{+\cdot}(S)_n$ and $SH^+(S)_m$. In other words, the clustering process provides more stabilization to SH^+ than it does $D^{+\cdot}$, which compensates for the unfavorable ΔGB of the reaction. Unfortunately, this hypothesis cannot be readily confirmed via calculation, since, to our knowledge, thermodynamic data specific to the formation of toluene radical cation clusters are unavailable. Qualitative arguments can, however, be made to rationalize the effect. For example, the extra stabilization provided the protonated methanol ions, relative to the toluene radical cations, is attributed to the strong hydrogen bonds that dipolar protonated methanol forms with other methanol molecules [16, 30], whereas the electrostatic binding of methanol to toluene photoions is relatively weak, due to the delocalized positive charge of the toluene ions. A similar argument could be made for the case of acetonitrile, since its protonated ions are also dipolar [31, 32]. Water, on the other hand, has a much lower GB value, and solvation effects appear to be insufficient to overcome the more unfavorable ΔGB of the reaction between it and toluene photoions, since this reaction is not observed [11].

Following the proton transfer reaction between dopant photoions and the solvent, an equilibrium distribution of protonated solvent clusters will rapidly be formed. The equilibrium constants for the successive clustering reactions

$$SH^+(S)_{n-1} + S \leftrightarrow SH^+(S)_n \quad \Delta G^\circ_{n-1,n}(SH^+) \tag{10}$$

are given by

$$K_{10} = \frac{n_{SH^+(S)_n}}{n_{SH^+(S)_{n-1}} \cdot p_S} \tag{11}$$

where p_S is the partial pressure of the solvent. Thus, the ratios between the number densities of the successive clusters are determined by the solvent number density (from which the p_S may be calculated) and by the equilibrium constants [15]. Thermodynamic data are available for protonated clusters of methanol [30] and acetonitrile [32], enabling calculation of the distribution of cluster sizes for a given n_S and temperature.

The protonated solvent clusters comprise the reagents for ionization of the analyte (M) via proton transfer:

$$SH^+(S)_n + M \leftrightarrow MH^+(S)_m + (1 + n - m)S \tag{12}$$

$$\Delta G^\circ_{12} = GB(S) - GB(M) + \Delta G^\circ_{0,m}(MH^+) - \Delta G^\circ_{0,n}(SH^+) = -RT\ln K_{12} \tag{13}$$

where the solvation energies for the protonated solvent and analyte are analogous to those defined by eq 9. From eq 13, clearly the spontaneity of analyte ionization reactions depends not just on the gas-phase basicities of the analyte and the solvent, but also on the solvation energies of their respective protonated ions. Some protonated analytes may form only weakly-bound clusters, especially carbon bases which do not provide a site of localized positive charge [14–16]. Presumably, steric hindrance will also inhibit solvation of analyte ions with bulky structures, if hydrogen bonding sites are blocked [33]. For these analytes whose ions form weakly-bound clusters, the cluster size distribution of the reagent ions is then an important factor which can affect ionization efficiency; depending upon ΔGB for the reaction, the larger solvent clusters may be unreactive, because of their higher solvation energies. This means that as the flow rate of solvent is increased, and the distribution of clusters is shifted towards larger sizes, the population of reagents capable of ionizing a species of fixed GB will be reduced. A lowering of the rate of analyte ion formation with an increase in solvent flow rate may thus be expected for analytes with relatively low gas-phase basicity and/or low solvation energy.

Ion Loss

Loss processes also occur within the DA-APPI source, limiting both the total ion current and the analyte ion current which may be delivered by the device. Knowledge of the loss processes operative in DA-APPI can be obtained from the literature of early API sources that utilized ^{63}Ni foils as the primary ionization means [34–37]. The ^{63}Ni API sources and this DA-APPI source share a common feature in that primary ionization and the ensuing reactions occur within a field-free region; consequently, separation of oppositely-charged species does not immediately occur within these sources. We then deduce that two loss processes are operative within the field-free region of the DA-APPI source: recombination of oppositely-charged species to form neutral products, and ambipolar diffusion of charged species to the walls. At the charge densities present within the DA-APPI source, recombination is believed to be the dominant loss process, since the rate of recombination is proportional to the product of both the positive and negative charged particle densities. Diffusion losses, meanwhile, are linear with charged particle density and are believed to have a relatively minor effect.

Within the photoionization region of the DA-APPI source, an equilibrium is established between primary ion formation, recombination loss, and transport of ions via vapor flow. Ignoring diffusion losses, the applicable steady-state rate equation is

$$\frac{dn_\pm}{dt} = \frac{R_P}{V} - \alpha \cdot n_\pm^2 - \frac{F}{V} \cdot n_\pm = 0 \tag{14}$$

where $n_\pm \equiv n_+ = n_-$ = the total number density of charge carriers of either polarity (cm^{-3}), R_P is the primary rate of photoion generation (ions s^{-1}), V = volume of the PI region (cm^3), α = recombination rate constant ($cm^3\ s^{-1}$), and F = total volumetric flow rate of the vapor ($cm^3\ s^{-1}$). A typical value for R_P is $\sim 3 \times 10^{12}$ ions s^{-1} (based upon a measured primary ion current of $\sim 0.5\ \mu A$ for toluene flow = 20 μl min^{-1}, methanol flow = 200 μl min^{-1}, and lamp current = 0.8 mA [27, 28]). The primary ions are assumed to be distributed uniformly throughout the cylindrical volume defined by the cross-sectional area of the vapor conduit (d = 0.7 cm), and the width of the intersecting photon beam (w $\approx$ 0.4 cm); thus, V $\approx$ 0.15 cm^3. For the sake of simplicity, following the example of Siegel and Fite [35], we assume a single universal recombination rate constant of about $10^{-6}\ cm^3\ s^{-1}$. A typical volumetric flow rate is $\sim 120\ cm^3\ s^{-1}$ (7.0 l min^{-1}). Substitution of these values into eq 14 enables the determination of the approximate steady-state concentration of charge carriers in the PI region: $n_\pm \approx 4 \times 10^9\ cm^{-3}$.

Downstream from the primary ionization region, the number density of charged particles decreases for the duration of the period in which the vapor resides within the field-free transport tube. Assuming no local anisotropy and only recombination losses, the number density of charged particles at any downstream position is given by [38],

$$n_\pm = \frac{n_0}{1 + n_0 \cdot \alpha \cdot t} \tag{15}$$

where n_0 is the number density of charge carriers in the

PI region, and t = time (s), calculated from the downstream distance divided by the linear velocity of the vapor. Assuming the oppositely-charged species of the vapor are abruptly separated at t = 10 ms (the actual time of separation depends on not only the volumetric flow rate, but also the field-penetration into the transport tube), and that no further losses occur, the terminal number density of ions in the vapor as it exits the transport tube is then $\sim 1 \times 10^8$ cm^{-3} for our example. Interestingly, this value is insensitive to the rate of primary ion production: primary photoion currents of 0.05, 0.5, 5, and 50 μA are calculated to yield terminal ion densities of 9.2, 9.8, 9.9, and 10×10^7 cm^{-3}, respectively. The recombination rate constant, however, has a large effect. For R_P = 0.5 μA, rate constants of 1, 2, 5, and 10×10^{-7} cm^3 s^{-1} are calculated to yield terminal ion densities of 9.2, 4.7, 1.9, and 1.0×10^8 cm^{-3}, respectively. Hence, diminishing returns in transmitted total ion current with increases in primary ion production are expected, because of the second-power dependence of recombination on charged particle density, with the asymptotic limit being a function of the recombination rate constant.

Balance Between Analyte Ion Production and Loss

A balance between analyte ion production via ion-molecule reactions and loss via recombination is maintained throughout the field-free region of the DA-APPI source. The steady-state rate equation for protonated analyte ions is

$$\frac{dn_{MH}}{dt} = k_{PT} \cdot n_M \cdot n_R - \alpha \cdot n_{MH} \cdot n_- = 0 \quad (16)$$

where n_{MH} is the number density of protonated analyte ions (cm^{-3}), k_{PT} is the forward rate constant for the proton transfer reaction (eq 12), n_M is the number density of neutral analyte molecules (cm^{-3}), n_R is the number density of reagent ions (cm^{-3}), and n_- is the total number density of negative charge carriers (cm^{-3}). Rearrangement yields an expression for the efficiency of the method:

$$\frac{n_{MH}}{n_M} = \left(\frac{k_{PT}}{\alpha}\right) \cdot \left(\frac{n_R}{n_-}\right) \quad (17)$$

Typical values for k_{PT} and α are about 10^{-9} and 10^{-6} cm^3 s^{-1}, respectively, so $k_{PT}/\alpha \approx 10^{-3}$. The ratio n_R/n_- will always be less than unity, because n_R is less than the total number density of positive charge carriers, n_+, and $n_- = n_+$. However, if the only positive charge carriers are reactive protonated solvent clusters and analyte ions, and if analyte ions make up a small fraction of the total, then $n_R/n_- \approx 1$. In this case, the ionization efficiency of the method is determined by the ratio k_{PT}/α, independent of the number density of reagent ions. Thus, even though recombination losses during the transport/reaction period severely deplete the population of reagent ions, the production of analyte ions may be unaffected (requires that the reagent ions remain in excess and that analyte ions lost to recombination reform analyte neutrals).

We previously discussed how increasing the solvent flow rate will shift the distribution of reagent ion clusters towards larger sizes. And, we noted that for those analytes with low gas-phase basicity and/or low solvation energy, the larger clusters may be unreactive. For these reasons, the ratio n_R/n_- will decrease for some analytes as the solvent flow rate is increased, to the extent that the population of reactive smaller solvent clusters is transformed into unreactive larger clusters. We then propose that a decrease in ionization efficiency, n_{MH}/n_M, due to a decrease in n_R/n_-, may be one mechanism responsible for the decline in DA-APPI sensitivity at higher solvent flow rates.

(Caveat: the DA-APPI source has a region in which the recombination loss mechanism is not operative—the space between the exit of the transfer tube and the inlet of the mass spectrometer. During the period in which ions from the tube travel towards the inlet, charge separation will have already occurred, and further ion-molecule reactions may proceed in the absence of recombination. The rate, and therefore the importance, of these additional reactions is believed to be low, however, because the number density of reagent ions will be at its lowest in this region.)

Results and Discussion

Dopant Only

We first examine the ion production of the PhotoSpray source when dopant alone is provided, in the absence of a sample stream. Figure 2 shows spectra acquired at toluene dopant flow rates of 0.2, 1, 5, and 20 μl min^{-1}. At 0.2 μl min^{-1}, the *m/z* 92 signal due to the toluene photoions is the base peak of the spectrum, and the only other prominent peak is at *m/z* 106. The *m/z* 106 peak is presumed due to ethylbenzene and/or xylene impurities in the liquid toluene that are ionized by charge exchange with the toluene photoions. As the toluene flow rate is increased, the *m/z* 92 signal increases to a maximum, then decreases, so that it is smaller at 20 μl min^{-1} than at 0.2 μl min^{-1}. At the same time, a number of new peaks gain prominence, which are attributed to additional, trace-quantity impurities introduced with the liquid toluene. The abundance of the primary photoions relative to that of background impurities is then continuously diminished as more liquid toluene is added, because, evidently, the photoions are increasingly consumed via reactions with the accompanying impurities.

We now examine the total yield of ions which may be obtained in the dopant-only case. Figure 3a shows plots of the TIC versus toluene dopant flow rate, for three lamp current settings. Figure 3b is a zoomed-in

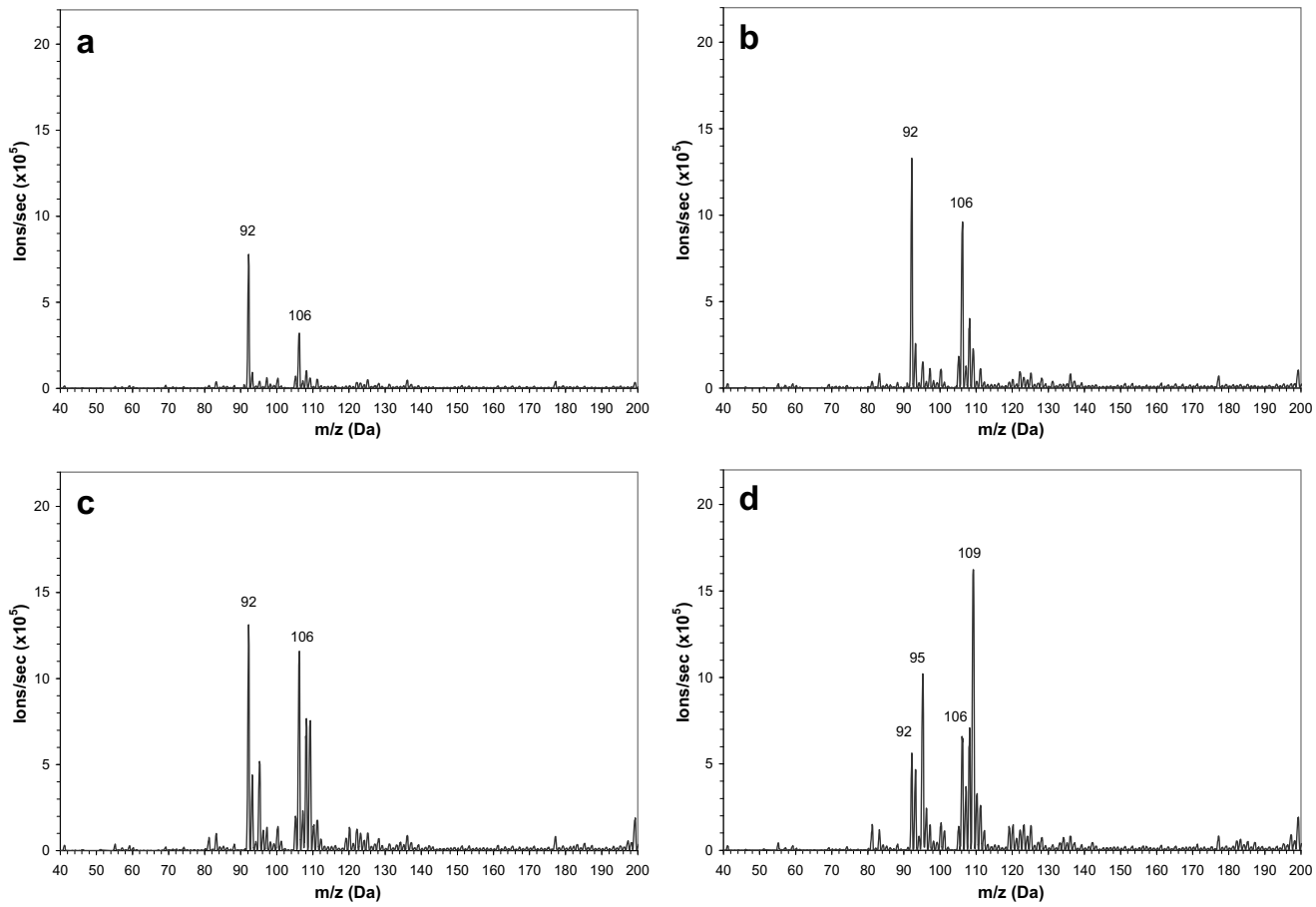

Figure 2. Spectra acquired with only toluene dopant being introduced into the source. (**a**)–(**d**) correspond to toluene flow rates of 0.2, 1, 5, and 20 μl min^{-1}, respectively.

display of the same results, showing details of the lower flow rate data. These plots show that the TIC in the absence of dopant or solvent flow is very low, and that a steep increase in the TIC occurs when the dopant flow is initiated. For each lamp current setting, the slope of the plot is regressive, continuously decreasing as the dopant flow rate is increased, until the TIC becomes nearly constant with further increases in dopant flow. Thus, there appears to be a limit to the TIC which can be obtained by increasing the dopant flow rate.

Regarding the effect of the lamp current, Figure 3 shows that raising the lamp current may also increase

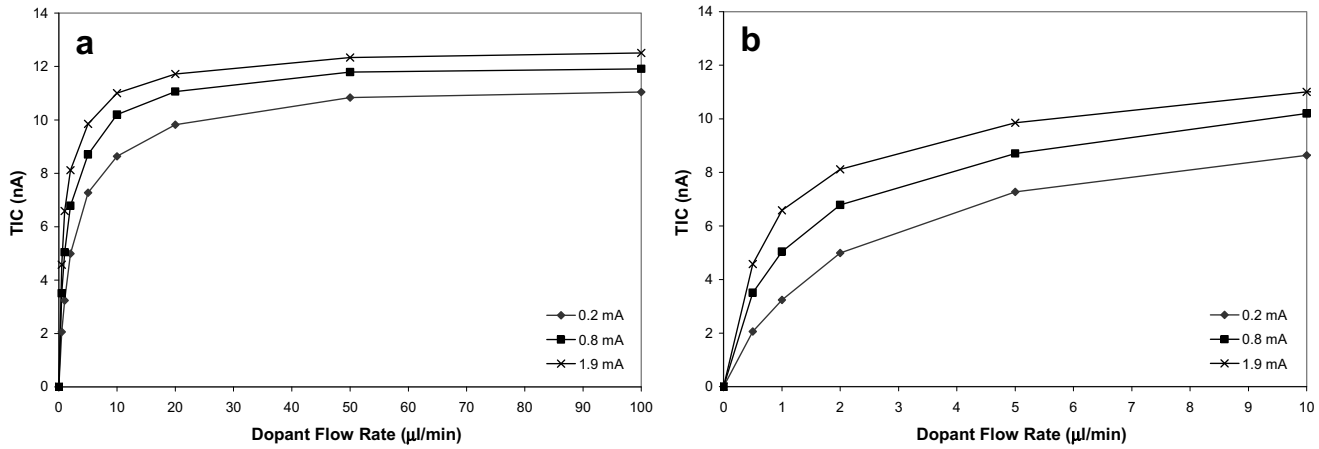

Figure 3. (**a**) Plots of the TIC, measured at the curtain plate versus toluene dopant flow rate, for three lamp current settings. No solvent is added. (**b**) A zoomed-in version of (**a**).

the TIC, but the effect is smaller at higher dopant flow rates. For example, by raising the lamp current from its lowest setting to its highest, 0.2 to 1.9 mA, the TIC at dopant flows of 1, 10, and 100 μl min^{-1} is increased by 103, 28, and 13%, respectively. Additional TIC versus lamp current results are plotted in Figure 4. These data confirm that the gains in TIC to be had by raising the lamp current are minimal at dopant flow rates at or above about 10 μl min^{-1}, and that the relative gains becomes smaller as the dopant flow is increased. Thus, the apparent limit in the TIC which can be obtained by increasing the dopant flow rate may not be substantially elevated by raising the lamp current.

We know that the observed near-plateau in deliverable TIC is not due to a limitation in the primary ionization rate, R_P. Our earlier experiments established that significant gains in primary photoion current can be obtained by raising the dopant flow rate, up to and above 100 μl min^{-1} [28]. These experiments also proved that raising the lamp current always increases the primary photoion current, regardless of the dopant flow rate. In the Theory section, however, we discussed how diminishing returns in TIC are expected, with increased primary ionization rate, because of the quadratic dependence of the recombination rate on charged-particle density (see eqs 14 and 15). The results in Figures 3 and 4 are consistent with this theory, since diminishing returns in TIC with increases in dopant flow and lamp current are in fact observed. Hence, we attribute the apparent limit in deliverable to TIC to the increased rate of neutralization via recombination that accompanies the increased production of primary photoions.

Quantitative comparisons between experiment and theory may also be attempted. With the exception of the recombination rate constant, α, the parameters required to calculate the terminal charged particle number density (using eqs 14 and 15), and thus the TIC, are known to a reasonable degree of certainty. Precise a priori determinations of α for our system are problematic, however, because of the complex, dynamic mixture of ions present (few of which have been positively identified) and the scarcity of recombination rate constant data. Another difficulty is the identities of the negative charge carriers are uncertain; electrons are initially produced, but these are rapidly scavenged by oxygen and other electron capturing impurities in the vapor, unless special cleaning steps are undertaken [36]. The best we can do now is then to work backwards and calculate the α required to yield the empirically-determined terminal $n_{\pm}$ values, and then to check if the α value is reasonable. For example, the TIC obtained at toluene flow = 100 μl min^{-1} and lamp current = 1.9 mA is ~13 nA, which corresponds to terminal $n_{\pm} \approx 7 \times 10^8$ cm^{-3}. Assuming R_P is ~5 μA (the measured value for similar conditions [28], we calculate the required α to be about 1.5×10^{7} cm^3 s^{-1}. According to Siegel [37], recombination rate constants for positive ions and thermal electrons are typically about 3×10^7 cm^3 s^{-1}, and sometimes an order of magnitude or more faster for heavily clustered ions, while positive ion-negative ion recombination rates may be comparable to, or even an order of magnitude slower, than positive ion-electron recombination rates. In the dopant-only case, the charged species are believed to be predominately unclustered positive ions and negative ions. Our calculated value for α is then within the (broad) range described by Siegel, so we can say at least that experiment and theory appear to be consistent in this regard.

In any event, the results in Figures 3 and 4 clearly show that the TIC approaches an asymptotic limit with increases in dopant flow and lamp current, the factors which govern the rate of primary ion generation, in qualitative agreement with theoretical expectations.

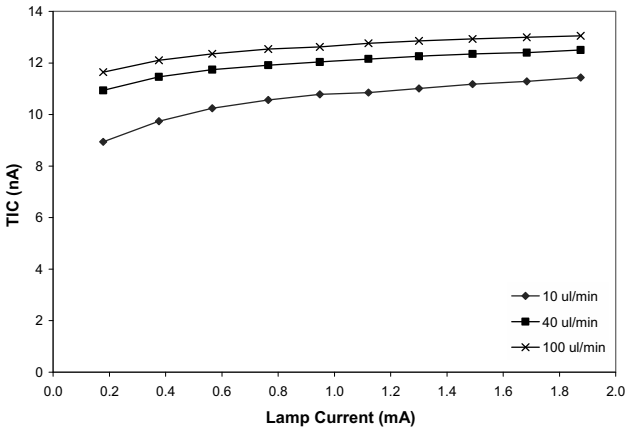

Figure 4. Plots of the TIC, measured at the curtain plate versus the lamp current, for three toluene dopant flow rates. No solvent is added.

Effect of Solvent

We now survey the effects of adding a liquid sample stream to the source. Figure 5 shows spectra obtained for the solvents and analytes utilized in these experiments. (Note these spectra do not accurately depict the true composition of the ions exiting the source reaction region, because ion-solvent clusters formed in the source experience irreversible loss of solvent during their passage through the dry curtain gas [14, 39].) Figure 5a and b are spectra of acridine in methanol and acetonitrile, respectively, showing its protonated molecular ion (MH^+) at m/z = 180, as well as a number of prominent background ions. Figure 5c and d are spectra of 9-MA in methanol and acetonitrile, showing MH^+ at m/z = 193, and in this case, significant quantities of $M^{+\cdot}$ at m/z = 192. No fragment ions from acridine or 9-MA are observed. Solvent-derived reagent ions are evident in all the spectra. For methanol, m/z = 51 and 65 are attributed to $(S + H_2O + H)^+$ and $(2S + H)^+$, whereas, for acetonitrile, m/z = 42, 60, and 83 are attributed to $(S + H)^+$, $(S + H_2O + H)^+$, and $(2S + H)^+$. The prominent background ions in the methanol spectra at m/z = 73, 87, and 101 have not been identified (we have observed

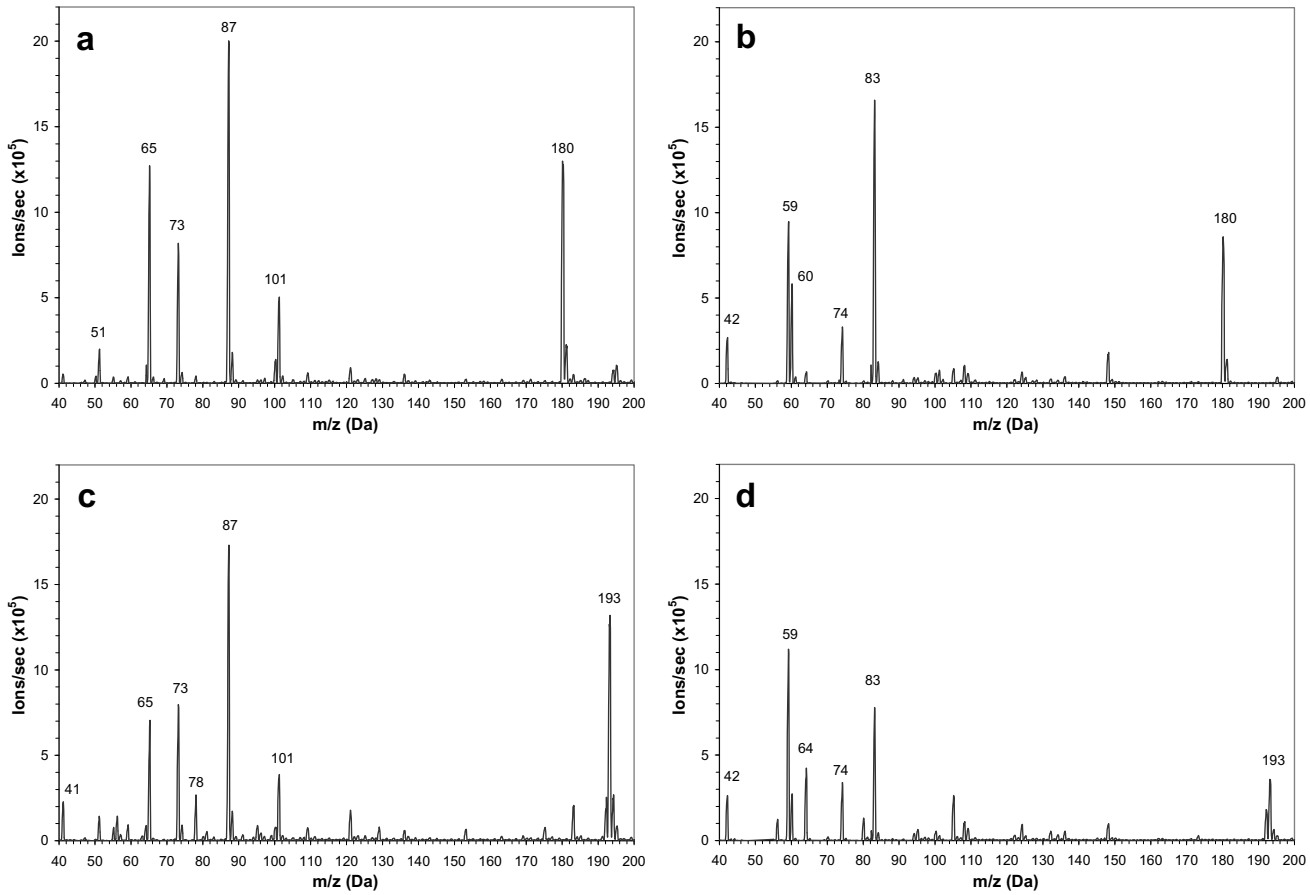

Figure 5. Spectra of the analytes and solvents used in these experiments. (**a**) and (**b**) are of acridine in methanol and acetonitrile, respectively, at heater T = 400 °C, while (**c**) and (**d**) are of 9-methylanthracene (9-MA) in methanol and acetonitrile, at heater T = 500 °C. The solvent flow is 200 μl min^{-1} and the toluene dopant flow is 20 μl min^{-1}.

that they can be eliminated by raising the solvent flow rate and/or lowering the heater temperature). The slight differences between the background spectra of acridine and 9-MA, for the same solvent, are the result of the different heater temperatures used for vaporization (400 °C for acridine, 500 °C for 9-MA). The higher temperature was found to improve the proton transfer ionization efficiency for 9-MA at higher solvent flow rates, though the same effect was not observed for acridine. Lastly, there are no prominent peaks in the spectra that are attributable to the toluene dopant. This shows that the toluene photoions do indeed react to near completion with both methanol and acetonitrile, under these conditions, and that the reagent ions used to transfer a proton to the analytes are derived primarily from the solvents.

Regarding the effect of solvent flow rate on analyte ionization efficiency, Figure 6a shows plots of acridine MH^+ signal versus methanol flow rate, for three fixed rates of toluene dopant introduction. Figure 6b shows plots of TIC versus solvent flow rate for the same conditions. Other than a slight increase at the lowest solvent flow rates, the general trend is for the MH^+ signal to decrease as the solvent flow is increased. The slightly depressed MH^+ signal at 25 and 50 μl min^{-1} is presumably due to incomplete conversion of dopant ions to protonated solvent ions. The spectra at methanol flows of 25 and 50 μl min^{-1} include many of the ions previously attributed to toluene impurities (results not shown); i.e., at low methanol flows, the spectra retain features of the dopant-only case (Figure 2). It appears then that the ions of toluene and its impurities are less favorable proton transfer reagents than protonated solvent ions, since the acridine MH^+ signal is depressed in their presence. For each toluene flow rate, the maximum MH^+ signal for acridine is obtained at methanol flows between 50 and 100 μl min^{-1}, and the sensitivity decreases by about half upon raising the methanol flow to 1000 μl min^{-1}. As for the effect of dopant flow, the data in Figure 6a show that the decline in sensitivity at higher solvent flow rates can be ameliorated somewhat by raising the toluene introduction rate from 10 μl min^{-1} to 50 or 100 μl min^{-1}, though there is no significant difference between 50 and 100 μl min^{-1}. Regarding the total yield of ions, Figure 6b indicates that there is a general, continuous decrease in the TIC as the solvent flow is increased, beginning with the first introduction of methanol. Like the trend in MH^+, the

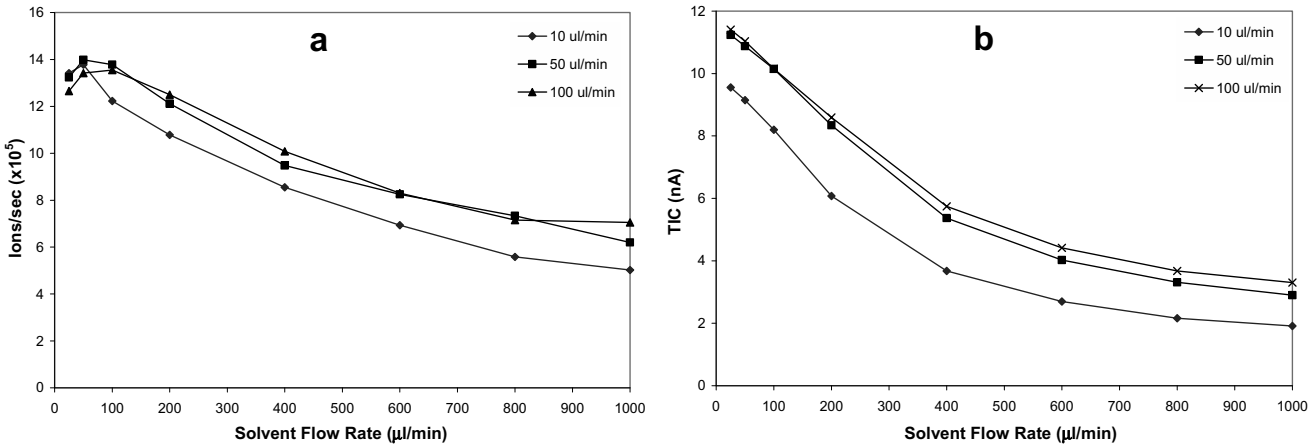

Figure 6. (**a**) Plots of the acridine MH^+ signal intensity versus methanol solvent flow rate, for three toluene dopant flow rates. (**b**) Plots of the TIC versus solvent flow rate, for the same conditions.

decrease in TIC with solvent flow can be partially offset by raising the dopant flow from 10 μl min^{-1} to higher values, though again, diminishing returns are obtained.

Additional results regarding the relationship between solvent flow, dopant flow, and the acridine MH^+ signal and the TIC, are presented in Figure 7a and b. In these experiments, the toluene dopant flow rates were set as percentages of the methanol solvent flow rate, for solvent flows of 50, 200, and 1000 μl min^{-1}. The plots in Figure 7 show the usual steep increases in analyte signal and TIC as the dopant flow is initiated, and they also confirm there are limits to the analyte signal which can be had by increasing the dopant flow. For each solvent flow rate, near plateaus in the signal are reached at dopant flows between 5–10% of the solvent flow. Since R_P is proportional to percent dopant under these conditions, these data demonstrate that beyond a certain point further increases in R_P do not significantly enhance the analyte ionization efficiency. One factor that contributes to this result is that diminishing returns in reagent ion concentration are obtained as R_P is increased, because of recombination, as evidenced by the regressive slopes of the plots in Figure 7b, and as previously discussed. It may also be that the reagent ion population is in excess; i.e., n_R/n_- of eq 17 is near unity, so that further increases in n_R have little effect (because they are matched by corresponding increases in n_-) and the ionization efficiency is mainly determined by the rate constants of proton transfer and recombination. At this juncture, we are unable to distinguish between the effects of these two mechanisms, since the trends in analyte signal and TIC with increases in percent dopant (and thus R_P) are similar.

The most important result from Figure 7a is that the decline in ionization efficiency with increases in solvent flow cannot be overcome by adding more dopant, since the apparent asymptote in signal at solvent flow = 1000 μl min^{-1} is about half that at 50 μl min^{-1}. As discussed in the Theory section, it is possible that the loss of sensitivity at higher solvent flow rates is due in part to

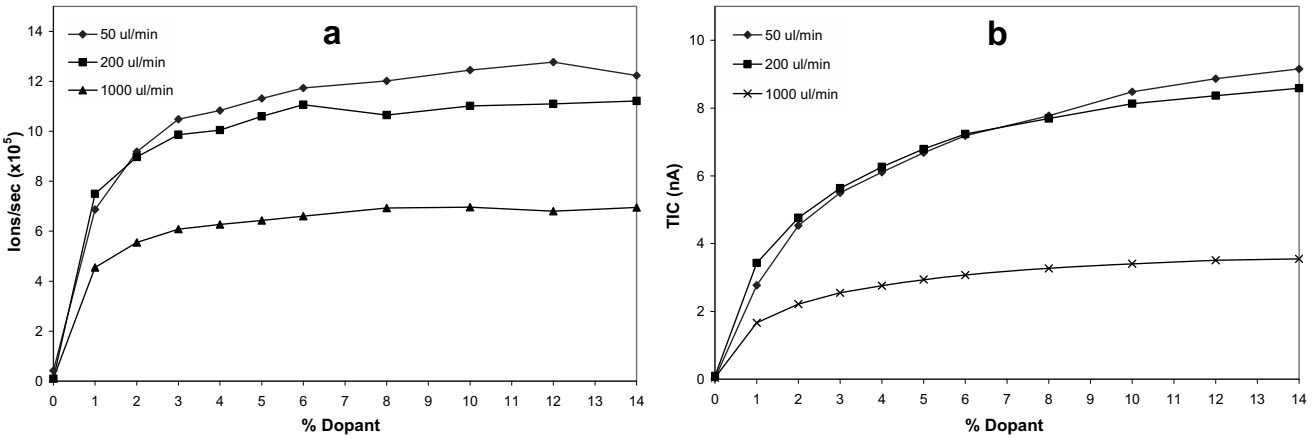

Figure 7. (**a**) Plots of the acridine MH^+ signal intensity versus toluene dopant flow rate (indicated as a percentage of the solvent flow), for three methanol solvent flow rates. (**b**) Plots of the TIC versus dopant flow rate, for the same conditions.

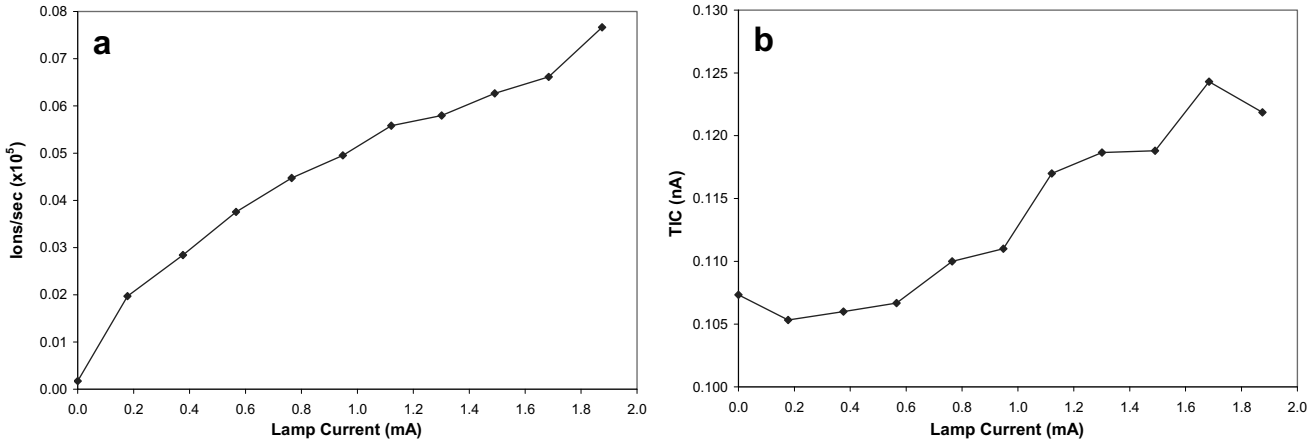

Figure 8. (**a**) Plot of the acridine MH^+ signal intensity versus lamp current, for methanol flow rate = 200 μl min^{-1}, *without dopant*. (**b**) Plot of the TIC versus lamp current, for the same conditions.

growth of the reagent ion clusters, because the larger clusters have greater solvation energies and may be unreactive (see eqs 12 and 13), which may result in a decline in n_R/n_- and thus, ionization efficiency (eq 17). However, this cannot be the only factor because it does not account for the substantial decrease in TIC; the apparent TIC limit of ~3 nA for methanol flow = 1000 μl min^{-1} is well below that measured in the absence of solvent, ~13 nA (Figure 3). In this case, the loss of TIC at higher solvent flow rates is definitely not due to a corresponding decrease in the primary ionization rate, because R_P can always be increased by adding more dopant or increasing the lamp current [27] and neither of these actions are able to restore the lost TIC (Figure 7b, and Figure 10, below). Instead, we suggest that another potential consequence of the growth of the reagent ion clusters with solvent flow is responsible for the lowering of the limits in both sensitivity and deliverable TIC. Specifically, we propose that the recombination rate constant, α, increases with the size of the ion-solvent clusters. We believe this is the only possible explanation for the decline in TIC with increased solvent flow, when R_P is constant (or increasing [27]) and the volumetric flow rate and temperature of the vapor are fixed. Further, this constitutes a second, more general mechanism by which analyte ionization efficiency may be lowered at higher solvent flow rates, in this case through a decline in k_{PT}/α (eq 17). Additional support for our hypothesis may be taken from an observation of Siegel: recombination rate constants are sometimes an order of magnitude, or more, faster for heavily clustered ions [37]. Siegel's comment, however, pertains to ion-electron recombination, and we cannot say with certainty that the same trends apply to ion-ion recombination. Summing up, the observed declines in sensitivity and TIC with increases in solvent flow rate are explainable by an accompanying increase in the recombination rate constant with cluster size, though more research is required to prove this hypothesis.

Effect of Lamp Current

We now take a closer look at the effect of the lamp current setting. Figure 8a and b show plots of acridine MH^+ signal and TIC versus lamp current, obtained *without dopant*, using a fixed methanol flow of 200 μl min^{-1}. In this case, the signal and TIC are both at least several hundred times lower than when dopant is added, and they both increase continuously with lamp current (though the TIC is near the detection limit of the measurement procedure, and thus noisy). These data demonstrate that the lamp current does in fact have a substantial effect on the primary rate of ion production, which might not have been obvious from the results presented so far. In our earlier experiments using the ionization detector, the primary ion current (and thus I_0) increased by 2.5 to 3 times when the lamp current was raised from 0.2 to 2 mA [28]. In Figure 8a, the same increase is observed in the signal, for about the same increase in lamp current. This tells us that the signal is proportional to I_0 under these conditions, even if this is not the case when dopant is provided. (As an aside, we note that recombination is not a significant process here, since for once, diminishing returns in signal with increases in R_P are *not* observed; indeed, for a TIC of ~20 pA, the terminal $n_\pm$ is about 10^6 cm^{-3} and recombination losses over the 10 ms transport period are calculated to be negligible.)

Figure 9a and b show plots of acridine MH^+ signal and TIC versus lamp current, for a range of toluene dopant flow rates (expressed as a percentage of the solvent flow rate), for methanol solvent flow = 200 μl min^{-1}. Figure 9c and d show the same results as Figure 9a and b, respectively, normalized to the values obtained at the highest lamp current setting. The results show that both the signal and TIC increase with lamp current, but the effect is smaller at higher dopant flows. The normalized plots show most clearly how the slopes in signal and TIC versus lamp current become less steep

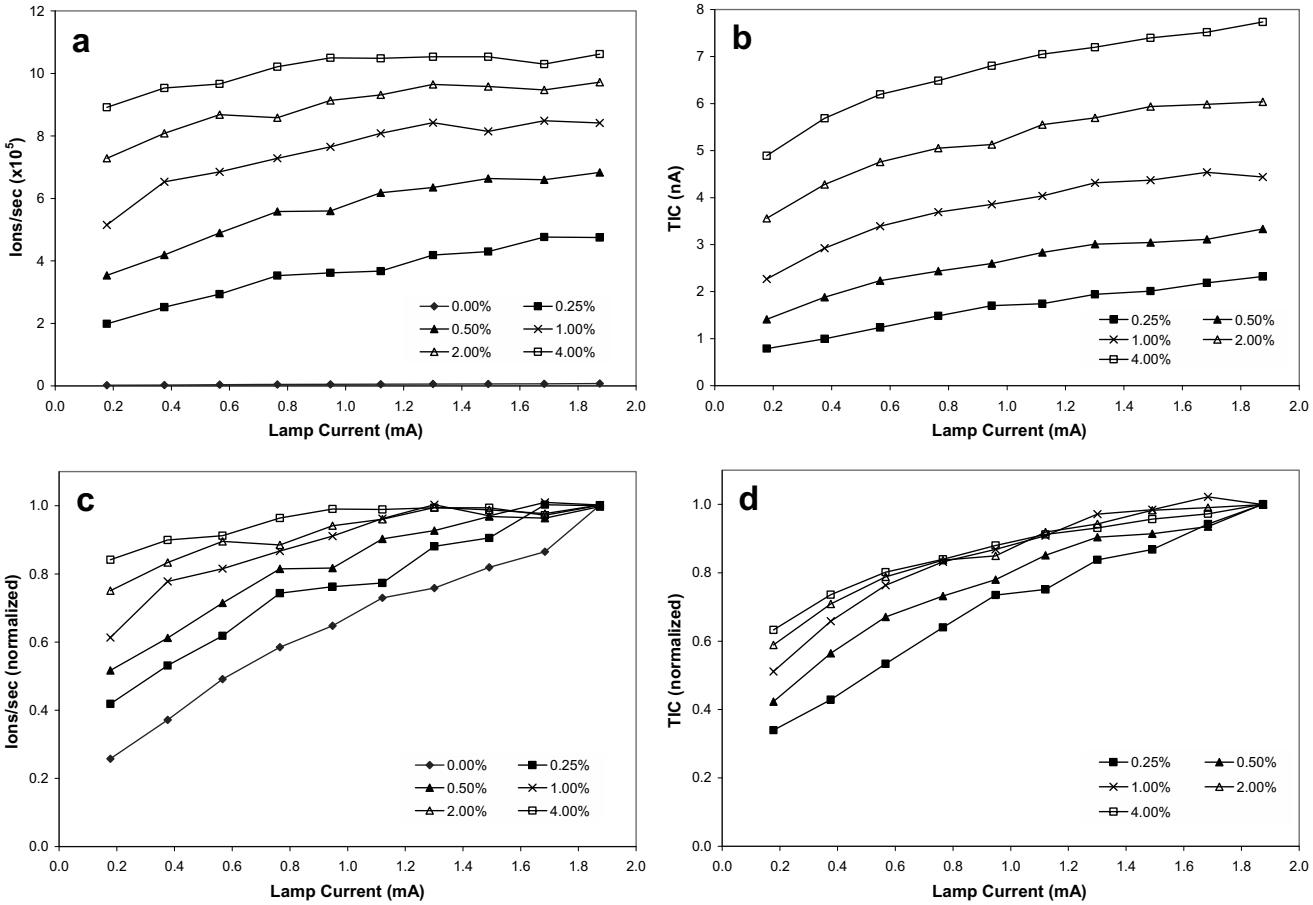

Figure 9. (**a**) Plots of the acridine MH^+ signal intensity versus lamp current, for a range of toluene dopant flow rates (indicated as a percentage of the solvent flow), with methanol solvent flow = 200 μl min^{-1}. (**b**) Plots of the TIC versus lamp current, for the same conditions. (**c**) and (**d**) The same as (**a**) and (**b**), respectively, but normalized to the values obtained at the highest lamp current.

as the dopant flow is raised. From theory (eqs 4 and 5), we expect that it should not matter if the requisite primary ion current is generated by using a relatively low dopant flow with a high lamp current, or a high dopant flow with a low lamp current, since either combination is predicted to yield the same results. The experimental results appear to support this conclusion, since the signal and TIC values obtained with lamp current = 0.2 mA and dopant flow = 4% are close to those obtained with lamp current = 1.9 mA (I_0 about 3.5 to 4 times that of the 0.2 mA case) and dopant flow = 1%. In practice, it is preferable to keep the lamp current setting at a moderate level and then to add more dopant as required, since the lifetime of the lamp is inversely proportional to the power at which it is operated (this assumes that the impurities introduced with the dopant do not adversely affect the analysis). Lastly, comparison of Figure 9c and d reveals that the signal does not vary as much as the TIC when the lamp current is raised, at the higher values of percent dopant; i.e., the extra TIC gained by raising the lamp current does not result in a proportional increase in signal. We take this as evidence supporting the theory that ionization efficiency becomes increasingly independent of the reagent ion concentration, as the reagent ions become increasingly in excess (eq 17).

Figure 10a and b show plots of acridine MH^+ signal and TIC versus lamp current, for methanol solvent flow rates of 50, 200, and 1000 μl min^{-1}, where the toluene dopant flow is set to 10% of the solvent flow. These data confirm that raising the lamp current has little effect under standard conditions, and that the losses in sensitivity and TIC with solvent flow rate cannot be overcome by adding more photons, in agreement with theory and our previous discussion.

Effect of Analyte

The final results regard the trends in ionization efficiency with solvent flow rate for different analytes, acridine and 9-MA, under standard conditions (dopant flow set to 10% of solvent flow, and lamp current = 0.8 mA). Figure 11a and b show plots of the MH^+ signal for acridine and 9-MA, respectively, versus solvent flow rate, for solvents methanol and acetonitrile. Figure 11a shows the by now familiar result that the sensitivity

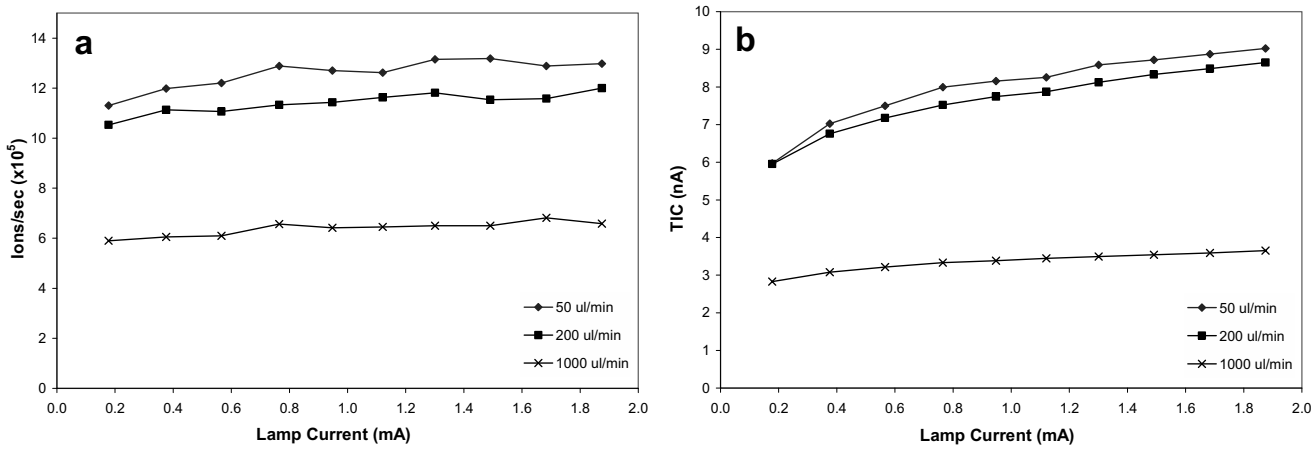

Figure 10. (**a**) Plots of the acridine MH^+ signal intensity versus lamp current, for methanol solvent flow rates of 50, 200, and 1000 μl min^{-1}. The toluene dopant flow is set to 10% of the solvent flow. (**b**) Plots of the TIC versus lamp current, for the same conditions.

towards acridine decreases gradually as the methanol flow is increased, and the signal at 1000 μl min^{-1} is about half that at the optimum flow (50–100 μl min^{-1}). A similar result is seen when the solvent is acetonitrile, though the sensitivity is somewhat diminished relative to the methanol case. Figure 11b, on the other hand, reveals a striking difference: unlike acridine, the 9-MA signal drops precipitously as the solvent flow is increased, until it effectively disappears above about 600 μl min^{-1} (the residual signal at higher flow rates is due mainly to the small background that was not subtracted). In this case, acetonitrile also provides less sensitivity than methanol. Control experiments demonstrated that the trends in the 9-MA signal with variations in dopant flow rate and lamp current are the same as those for acridine, so the decline in sensitivity for 9-MA with increased solvent flow cannot be overcome by increasing the values of these parameters. We attribute the contrast between the results for acridine and 9-MA to differences in both their gas-phase basicities and solvation energies. Specifically, 9-MA has a relatively low GB value, and it is a carbon base (so its solvation energy is also relatively low), which means that 9-MA is less able than acridine (high GB, nitrogen base) to undergo proton transfer reactions with the larger protonated solvent clusters with their high solvation energies (see eqs 12 and 13). Note that when the solvent flow rate is around 100 μl min^{-1}, the 9-MA sensitivity is fairly high, indicating that the proton transfer reaction between it and the smaller solvent cluster ions is exoergic and favored. At the higher solvent flows, apparently, the growth in size of the solvent cluster ions, and the attendant increase in their solvation energies, reduces the population of reagents capable of ionizing 9-MA, with the ultimate result that the rate of analyte ion formation, and hence the sensitivity, is diminished. Conversely, acridine's high GB and (presumably relatively high) solvation energy com-

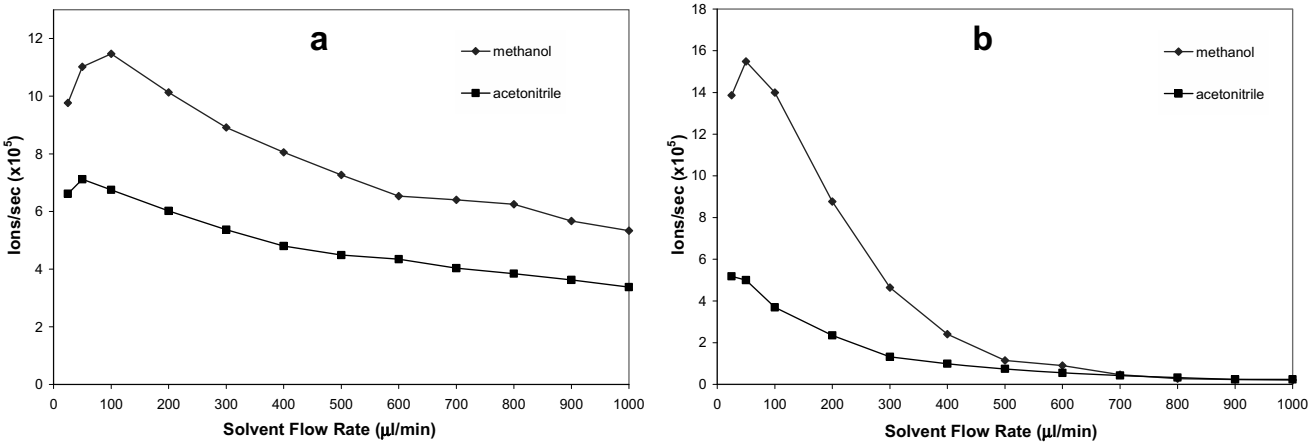

Figure 11. (**a**) Plots of the MH^+ signal for acridine versus solvent flow rate, for solvents methanol and acetonitrile. Standard conditions were utilized (the toluene dopant flow is set to 10% of the solvent flow, and the lamp current is 0.8 mA). (**b**) The same as (**a**), but the analyte is 9-methylanthracene (9-MA) and a heater temperature of 500 °C was used (instead of 400 °C).

bine to render exothermic the proton transfer reaction between it and the solvent clusters for even the highest solvent flow tested, since the decline in sensitivity observed for acridine is relatively small (and explainable in part by the deduced increase in the recombination rate). These results, then, substantiate the theory that proton transfer ionization efficiency, n_{MH}/n_M, is adversely affected by increases in the solvent flow for those analytes with relatively low gas-phase basicity and/or solvation energy, evidently because of a decrease in n_R/n_- with increases in cluster size.

Conclusions

The results of this investigation demonstrate that there are limits to the sensitivity which can be obtained by increasing the dopant flow rate and the power of the discharge lamp, two factors which govern the primary rate of dopant ion generation in DA-APPI. Theory and supporting experimental evidence indicate that the recombination loss process plays a dominant role in determining both the maximum deliverable total ion current and the analyte ionization efficiency. The results also show that the ionization efficiency of DA-APPI is diminished at higher solvent flow rates, regardless of the primary ionization rate. Empirical evidence suggests that this is in part due to an increase in the recombination rate constant with solvent flow, which is itself believed to be a result of the accompanying growth in size of the ion-solvent clusters. However, the loss of sensitivity with increase in solvent flow is also compound-dependent: for acridine, a nitrogen base having high gas-phase basicity, only a minor loss of sensitivity occurs upon increasing the solvent flow to 1 ml min^{-1}; for 9-methylanthracene, a carbon base having relatively low gas-phase basicity, increasing the solvent flow to 1 ml min^{-1} results in a complete loss of sensitivity. The loss of sensitivity for 9-MA is attributed to another consequence of the growth in size of the ion-solvent clusters within the source: the high solvation energies of the larger protonated-solvent clusters render them unreactive towards analytes with low gas-phase basicity and/or low solvation energy. Thus, the results indicate that analyte ionization efficiency can be affected by ion-solvent cluster growth at higher solvent flow rates through two mechanisms: the larger protonated solvent clusters have higher solvation energies and are less likely to undergo proton transfer reactions, and, apparently, larger clusters are more likely to be neutralized through recombination. The relative importance of each mechanism will be compound dependent.

Acknowledgments

The authors extend special thanks to Peter Jacob of NV Organon (Oss, the Netherlands) for the kind donation of the Photospray ion source. The authors acknowledge David Chen and Don Douglas of the University of British Columbia (UBC) for providing access to the mass spectrometer. They acknowledge the Natural Sciences and Engineering Research Council of Canada and UBC for financial support.

References

1. Yamashita, M.; Fenn, J. B. Electrospray Ion Source. Another Variation on the Free-Jet Theme. *J. Phys. Chem.* **1984,** *88,* 4451–4459.
2. Bruins, A. P.; Covey, T. R.; Henion, J. D. Ion Spray Interface for Combined Liquid Chromatography/Atmospheric Pressure Ionization Mass Spectrometry. *Anal. Chem.* **1987,** *59,* 2642–2646.
3. Carroll, D. I.; Dzidic, I.; Stillwell, R. N.; Haegele, K. D.; Horning, E. C. Atmospheric Pressure Ionization Mass Spectrometry: Corona Discharge Ion Source for Use in Liquid Chromatograph-Mass Spectrometry Computer Analytical System. *Anal. Chem.* **1975,** *47,* 2369–2373.
4. Henion, J. D.; Thomson, B. A.; Dawson, P. H. Determination of Sulfa Drugs in Biological Fluids by Liquid Chromatography/Mass Spectrometry/Mass Spectrometry. *Anal. Chem.* **1982,** *54,* 451–456.
5. Robb, D. B.; Covey, T. R.; Bruins, A. P. Atmospheric Pressure Photoionization: An Ionization Method for Liquid Chromatography-Mass Spectrometry. *Anal. Chem.* **2000,** *72,* 3653–3659.
6. Syage, J. A.; Evans, M. D.; Hanold, K. A. Photoionization Mass Spectrometry. *Am. Lab.* **2000,** *32,* 24–29.
7. Raffaelli, A.; Saba, A. Atmospheric Pressure Photoionization Mass Spectrometry. *Mass Spectrom. Rev.* **2003,** *22,* 318–331.
8. Hsieh, Y.; Wang, G. Integration of Atmospheric Pressure Photoionization Interfaces to HPLC-MS/MS for Pharmaceutical Analysis. *Am. Pharm. Rev.* **2004,** *7,* 88–93.
9. Koster, G.; Bruins, A. P. Mechanisms for Ion Formation in LC/MS by Atmospheric Pressure Photo-Ionization (APPI). *Proceedings of the 49th ASMS Conference on Mass Spectrometry and Allied Topics*; Chicago, IL, May, 2001.
10. Rauha, J.-P.; Vuorela, H.; Kostiainen, R. Effect of Eluent on the Ionization Efficiency of Flavonoids by Ion Spray, Atmospheric Pressure Chemical Ionization, and Atmospheric Pressure Photoionization Mass Spectrometry. *J. Mass Spectrom.* **2001,** *36,* 1269–1280.
11. Kauppila, T. J.; Kuuranne, T.; Meurer, E. C.; Eberlin, M. N.; Kotiaho, T.; Kostiainen, R. Atmospheric Pressure Photoionization Mass Spectrometry. Ionization Mechanism and the Effect of Solvent on the Ionization of Naphthalenes. *Anal. Chem.* **2002,** *74,* 5470–5479.
12. Kauppila, T. J.; Kotiaho, T.; Kostiainen, R.; Bruins, A. P. Negative Ion-Atmospheric Pressure Photoionization Mass Spectrometry. *J. Am. Soc. Mass Spectrom.* **2004,** *15,* 203–211.
13. Kauppila, T. J.; Kostiainen, R.; Bruins, A. P. Anisole, a New Dopant for Atmospheric Pressure Photoionization Mass Spectrometry of Low Proton Affinity, Low Ionization Energy Compounds. *Rapid Commun. Mass Spectrom.* **2004,** *18,* 808–815.
14. Sunner, J.; Nicol, G.; Kebarle, P. Factors Determining Relative Sensitivity of Analytes in Positive Mode Atmospheric Pressure Ionization Mass Spectrometry. *Anal. Chem.* **1988,** *60,* 1300–1307.
15. Sunner, J.; Ikonomou, M. G.; Kebarle, P. Sensitivity Enhancements Obtained at High Temperatures in Atmospheric Pressure Ionization Mass Spectrometry. *Anal. Chem.* **1988,** *60,* 1308–1313.
16. Nicol, G.; Sunner, J.; Kebarle, P. Kinetics and Thermodynamics of Protonation Reactions: $H_3O^+(H_2O)_h + B = BH^+(H_2O)_b + (h - b + 1)H_2O$, where B is a Nitrogen, Oxygen, or Carbon Base. *Int. J. Mass Spectrom. Ion Processes* **1988,** *84,* 135–155.

17. Robb, D. B.; Bruins, A. P.; Peters, H. A. M.; Jacobs, P. L. Atmospheric Pressure Photoionization (APPI) for High Sensitivity LC/MS in Bioanalysis. *Proceedings of the 48th ASMS Conference on Mass Spectrometry and Allied Topics*; Long Beach, CA, June, 2000.
18. Robb, D. B., Bruins,, A. P. University of Groningen, the Netherlands, 1998–2000, unpublished results.
19. Yang, C.; Henion, J. Atmospheric Pressure Photoionization Liquid Chromatographic-Mass Spectrometric Determination of Idoxifene and Its Metabolites in Human Plasma. *J. Chromatogr. A.* **2002,** *970,* 155–165.
20. Hsieh, Y.; Merkle, K.; Wang, G.; Brisson, J.-M.; Korfmacher, W. A. High-Performance Liquid Chromatography-Atmospheric Pressure Photoionization/Tandem Mass Spectrometric Analysis for Small Molecules in Plasma. *Anal. Chem.* **2003,** *75,* 3122–3127.
21. Kauppila, T. J.; Kostiainen, R.; Bruins, A. P. Effect of the Flow Rate on the Ionization Efficiency in Atmospheric Pressure Photoionization Mass Spectrometry. *Proceedings of the 51st ASMS Conference on Mass Spectrometry and Allied Topics*; Montreal, Canada, June, 2003.
22. SCIEX° *PhotoSpray Ion Source Operator's Manual*;° December 2002.
23. http://www.cathodeon.com/articles/article1.htm.
24. http://webbook.nist.gov/chemistry.
25. Chupka, W. A. Ion-Molecule Reactions by Photoionization Techniques. In *Ion-Molecule Reactions, Vol. I*; Franklin, J. L., Ed.; Plenum Press: New York, NY, 1972; pp 33–76.
26. De Wit, J. S. M.; Jorgenson, J. W. Photoionization Detector for Open-Tubular Liquid Chromatography. *J. Chromatogr.* **1987,** *411,* 201–212.
27. Robb, D.; Blades, M. Studies of the Factors Governing Ion Current Production for the Dopant-Assisted Atmospheric Pressure Photoionization (DA-APPI) Source for LC/MS. *Proceedings of the 52nd ASMS Conference on Mass Spectrometry and Allied Topics*; Nashville, TN, May, 2004.
28. Robb, D.; Blades, M., unpublished results.
29. Su, T.; Bowers, M. T. Classical Ion-Molecule Collision Theory. In *Gas Phase Ion Chemistry; Vol. I*; Bowers, M. T., Ed.; Academic Press: New York, NY, 1979; p 96.
30. Meot-Ner (Mautner), M. Comparative Stabilities of Cationic and Anionic Hydrogen-Bonded Networks. Mixed Clusters of Water-Methanol. *J. Am. Chem. Soc.* **1986,** *108,* 6189–6197.
31. Meot-Ner (Mautner), M. Solvation of the Proton by HCN and CH_3CN. Condensation of HCN with Ions in the Gas Phase. *J. Am. Chem. Soc.* **1978,** *100,* 4694–4699.
32. Deakyne, C. A.; Meot-Ner (Mautner), M.; Campbell, C. L.; Hughes, M. G.; Murphy, S. P. Multicomponent Cluster Ions. 1. The Proton Solvated by CH_3CN/H_2O. *J. Chem. Phys.* **1986,** *84,* 4958–4969.
33. Grimsrud, E. P.; Kebarle, P. Gas Phase Ion Equilibria Studies of the Solvation of the Hydrogen Ion by Methanol, Dimethyl Ether, and Water. Effect of Hydrogen Bonding. *J. Am. Chem. Soc.* **1973,** *95,* 7939–7943.
34. Carroll, D. I.; Dzidic, I.; Stillwell, R. N.; Horning, M. G.; Horning, E. C. Subpicogram Detection System for Gas Phase Analysis Based upon Atmospheric Pressure Ionization (API) Mass Spectrometry. *Anal. Chem.* **1974,** *46,* 706–710.
35. Siegel, M. W.; Fite, W. L. Terminal Ions in Weak Atmospheric Pressure Plasmas. Applications of Atmospheric Pressure Ionization to Trace Impurity Analysis in Gases. *J. Phys. Chem.* **1976,** *80,* 2871–2881.
36. Siegel,° M.° W.;° McKeown,° M.° C.° Ions° and° Electrons° in° the Electron Capture Detector. Quantitative Identification by Atmospheric Pressure Ionization Mass Spectrometry. *J. Chromatogr.* **1976,** *122,* 397–413.
37. Siegel, M. W. Atmospheric Pressure Ionization. In *Plasma Chromatography*; Carr, T. W., Ed.; Plenum Press: New York, NY, 1984; pp 95–113.
38. Loeb, L. B. The Recombination of Ions. In *Basic Processes of Gaseous Electronics*; University of California Press: Berkeley, CA, 1955; p 478.
39. Bruins, A. P. ESI Source Design and Dynamic Range Considerations. In *Electrospray Ionization Mass Spectrometry*; Cole, R. B., Ed.; John Wiley and Sons: New York, NY, 1997, pp 107–136.